

A novel approach to generate datasets with XAI ground truth to evaluate image models

Miquel Miró-Nicolau^{a,b,*}, Antoni Jaume-i-Capó^{a,b}, Gabriel Moyà-Alcover^{a,b}

^a*UGiVIA Research Group, University of the Balearic Islands, Dpt. of Mathematics and Computer Science, 07122 Palma (Spain)*

^b*Laboratory for Artificial Intelligence Applications (LAIA@UIB), University of the Balearic Islands, Dpt. of Mathematics and Computer Science, 07122 Palma (Spain)*

Abstract

With the increased usage of artificial intelligence (AI), it is imperative to understand how these models work internally. These needs have led to the development of a new field called eXplainable artificial intelligence (XAI). This field consists of on a set of techniques that allows us to theoretically determine the cause of the AI decisions. One unsolved question about XAI is how to measure the quality of explanations. In this study, we propose a new method to generate datasets with ground truth (GT). These datasets allow us to measure how faithful is a method without ad hoc solutions. We conducted a set of experiments that compared our GT with real model explanations and obtained excellent results confirming that our proposed method is correct.

Keywords: Fidelity, Explainable Artificial Intelligence (XAI), Objective evaluation

PACS: 0000, 1111

2000 MSC: 0000, 1111

1. Introduction

The increased use of neural networks in various field has led to new challenges. One is the difficulty in understanding the causes of their results. This

*Corresponding author

Email addresses: miquel.miro@uib.es (Miquel Miró-Nicolau), antoni.jaume@uib.es (Antoni Jaume-i-Capó), gabriel.moya@uib.es (Gabriel Moyà-Alcover)

limitation was addressed by eXplainable artificial intelligence (XAI), which solves the black-box nature of these models.

XAI algorithms have become a major field of study. In particular, it has been widely used in sensitive fields such as medical praxis, as can be seen in the recent publication of studies that reviewed the existing state-of-art of XAI methods applied to medical images ([9], [15]). From these studies, two conclusions can be drawn. First, different XAI techniques significantly different results about the quality of all XAI algorithms. Second, there is a lack of objective metrics to measure the quality of explanations. These two conclusions can be extended to any XAI method for image analysis, as assessed by Miller [8] *most of the work about explainability relies on the authors' intuition, and an essential point is to have metrics that describe the overall explainability with the aim to compare different models regarding their level of explainability*. Similarly, Tomsett *et al.* [14] also identified the need to measure the quality of the explanation, in conjunction with a set of other requirements that should be fulfilled to obtain a valid explanation. Tomsett *et al.* [14] identified fidelity as a property of an explanation corresponding to its quality. Fidelity, or faithfulness, is a property that indicates how well an explanation *represents the processing performed by a model on the input to produce the corresponding output*. Thus, a correct XAI pipeline, a part of to obtain the explanation, should measure its faithfulness.

Alvarez *et al.* [1] stated that fidelity measurement is difficult because *assessing the correctness of estimated feature relevance requires a reference "true" influence to compare against and this is rarely available*. These limitations have led to a lack of consensus on measuring faithfulness. Various authors proposed different methods for measuring it.

A relevant number of methods ([13], [10], [1]) aim to measure faithfulness by assuming that the overall performance of an Artificial Intelligence (AI) model must significantly change without the most important input features. The absence of these important features is produced by the perturbation of the original input. Samek *et al.* [13] defined perturbation as the iterative process of removing information from the input data. They proposed removing the information in a specific order, from more to less important (most relevant first, abbreviated as MoRF). This iterative process generates a curve and Samek *et al.* proposed the area over this perturbation curve (AOPC) to measure fidelity. Similar to Samek *et al.*, Petsiuk *et al.* [10] proposed the area over the curve as a metric. The main difference is that they proposed adding relevant information as an alternative metric. Alvarez-Melis *et al.* [1]

proposed to calculating the correlation between the score variation, when a region is deleted and the importance of the region according to the XAI algorithm.

The faithfulness measures analysed so far have multiple caveats. Adding these measurements increase the complexity of the AI pipeline. These measures were all difficult to calculate, which new set of problems. Similar to XAI methods, we found that different faithfulness metrics yielded different results. Furthermore, as stated by Gomez *et al.* [4] and Qiu *et al.* [11], the results could not be directly used because none of the measures considered the out-of-domain (OOD) problem. Gomez *et al.* [4] and Qiu *et al.* [11] proposed solutions to these limitations by adding a new layer of complexity. These new complexity increase the possibility of new errors.

Recently, a set of studies have attempted to address these limitations ([3], [2] and [7]). These authors proposed to generate artificial datasets with ground truth for the explanations. These datasets allowed us to measure the fidelity of the methods directly without adding new sources of problems. Cortez and Embrechts [3] proposed a new XAI method and used a synthetic dataset as a benchmark. The dataset was a set of 1000 different samples of four random values- i.e. the author built a dataset of tabular data. This dataset, in addition to the four random samples, contained a synthetic label. This label was built using a weighted sum of the data from the dataset. An AI model was trained to regress this synthetic label from the data. The resultant model weights each feature of the dataset with the weights of the sum that generates the label. These weights represent the ground truth of the explanation. Cortez and Embrechts [3] obtained a ground truth for the explanation; for this reason, they could measure the exact fidelity of the XAI method. Nonetheless, their proposal had two apparent limitations: they only applied to regression problems and for tabular data. Arras *et al.* [2] proposed a methodology for generating a synthetic attribution dataset of images. The proposed methodology was based on visual question answering (VQA) models. These models are specific types of AI model that can answer questions regarding the content of an image. Arras *et al.* [2] proposed asking questions depending only on one object from the image. They consider an explanation correct if only the object of interest in the question was highlighted. Following this methodology, they compared 11 different XAI methods. Arras *et al.* proposal was capable to handle images data. Nevertheless, only in a very specific problem, the VQA models. They also did not consider the importance value of the explanations; instead, they only considered the

position of the most important elements. Mamalakis *et al.* [7] made two main contributions: On the one hand, they named this type of datasets *synthetic attribution benchmark* and formalized them. They defined them as the conjunction of three elements: *synthetic input X , function F and synthetic output Y , the latter is the result of applying F to X* . However, the methodology they proposed was used for classification problems, as shown by their synthetic attribution benchmark. X of this dataset is a set of binary images of circles and squares. Y was one of two classes: the first one indicated more area of circles than squares, and the second indicated the contrary. With this information, they compared 12 methods. All 12 methods indicate the positive or negative of each pixel in a given class. Mamalakis *et al.* [7] proposal can be used for classification models, but it only verifies whether the features have a negative or positive impact on the classification. Similar to Arras *et al.* [2], did not consider the value of the explanation.

We proposed a new methodology based on the work of Cortez and Embrechts [3] to build synthetic attribution benchmark datasets with a defined GT for image tasks. This dataset allows evaluation of the fidelity of an XAI method. Our goal is to overcome the limitation of the other proposals. We identified two limitations on the existing state-of-art, not considering the value of the explanation and being unable to use it for most typical image-related tasks. With our methodology, we use the exact explanation value as GT we can use indistinctly for regression and classification.

The rest of this paper is organized as follows. In the next section, we describe our methodology for building synthetic attributions benchmarks. In Section 3, we specify the experimental environment, and we describe the datasets, measures, metrics, and predictive models used for experimentation. Section 4 discuss the results and comparison experiments obtained after applying the two datasets generated using the proposed method to multiple common XAI methods. Finally, in Section 5 we present the conclusions of the study.

2. Method

We based our proposal on the work of Cortez and Embrechts [3]. As explained in the previous section, these authors generated a synthetic attribution benchmark (SAB) for tabular data. The proposed methodology enhances their method and applies it to images. Similar to the original work, we used it for regression, but also for classification tasks. This was accom-

plished by changing how the label was generated. Instead of tabular features, we proposed to use numerical information found on the images, such as the number of times a pattern was found on an image.

To define our methodology, we use the formalization of SAB proposed by Mamalakis *et al.*. We set three different elements: the input data \mathcal{X} , attribution function F , and output data \mathcal{Y} . This was conducted as follows:

Input data: In this step, we defined the input data, which is a collection of n images: $\mathcal{X} = \{I_1, I_2, \dots, I_n\}$. In each image, we can find multiple occurrences of different patterns $p \in \mathcal{C}$, where \mathcal{C} is the set of all possible features that can be identified in an image. The definition of p is strongly related to the nature of the experiment. In figure 1, for example, we have six different p , $\mathcal{C} = \{ \text{circles, crosses, uniform figures, blue texture figures, uniform circles, uniform crosses, blue texture circles, and blue texture crosses} \}$. However, depending on the problem definition only a subset of \mathcal{C} is considered.

Attribution function. We define a function $F : \mathcal{X} \rightarrow \mathbb{R}$. This function takes an image I and uses the p present on it, $F(I) = \sum_{i=1}^m w_i \cdot g(p_i, I)$, where m is the total number of different p considered, $g(p_i, I)$ is a function that extracts some information of the pattern p_i of the image I , for example the number of times that this pattern appears on the image, and w_i is the ground truth for the importance of pattern p_i for image I .

To adapt this function to a binary classification task, it must be altered. The output must have only two possible values. This behaviour was accomplished using the step function, $F_{\text{classification}}(I) = F(I) \leq 0$.

Output:. We generated labels, or output data, by combining the function and input data. When \mathcal{X} and F are defined, the output data is $\mathcal{Y} = \{y : \forall I \in \mathcal{X}, y \Rightarrow F(I)\}$.

In the following section, we describe the experimental setup used to test whether this methodology allowed us to analyse the quality of a given XAI method.

3. Experimental setup

The end-goal of the experimental setup was to verify whether the ground truth, generated by the proposed methodology corresponded to the actual explanations. To determine whether this was the case, we conducted multiple experiments. To do these experiments, we needed an XAI method as a proxy to obtain explanations. We need to trust that the results of the XAI method were faithful to the learned relations of the predictive model.

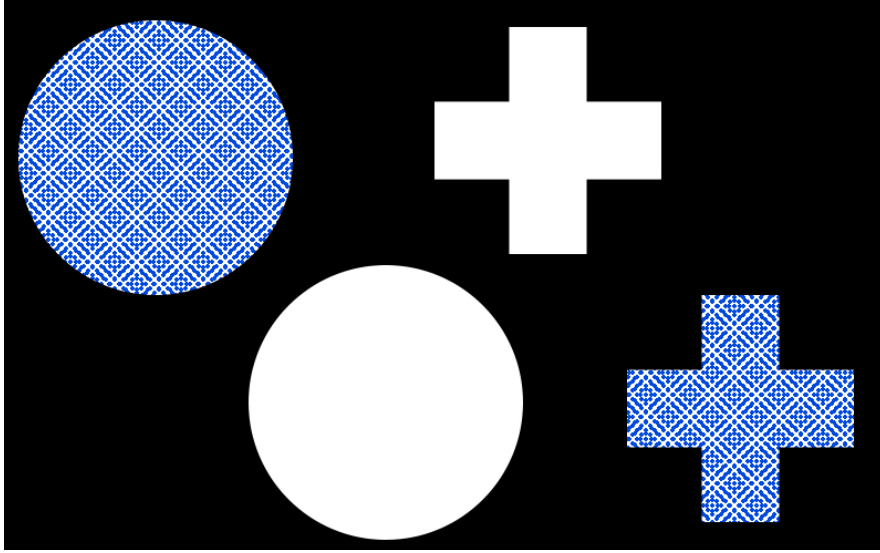


Figure 1: Image containing different patterns. The total amount of patterns presented in the image is $|C| = 6$. Nonetheless, depending on the problem, only a subset of this C is considered, e.g., if the problem is based on texture analysis, we have two different p , the uniform elements and the ones containing the blue texture.

3.1. Datasets

Following the proposed methodology, we generated two different datasets: AIXI-Shape (Artificial Intelligence eXplainable Insights) and AIXI-Color. These datasets consist of 50000 images for training and 2000 for validation. All images had a size of 128 pixels per 128 pixels. We used this image size to simplify the training process. Both the datasets and scripts used to generate them are available at <https://github.com/miquelmn/aixi/releases/tag/1.0.0>.

Each dataset allowed us to assess whether the proposed methodology was accurate in different environments. In particular, we investigated whether the method was correct for patterns of different natures (colours and shapes).

3.1.1. AIXI-Shape

The images from AIXI-Shape were built using a combination of three different patterns: circles, squares, and crosses, as shown in figure 2a. We used these forms for the different types of visual patterns. We used these simple forms because they are easily recognizable.

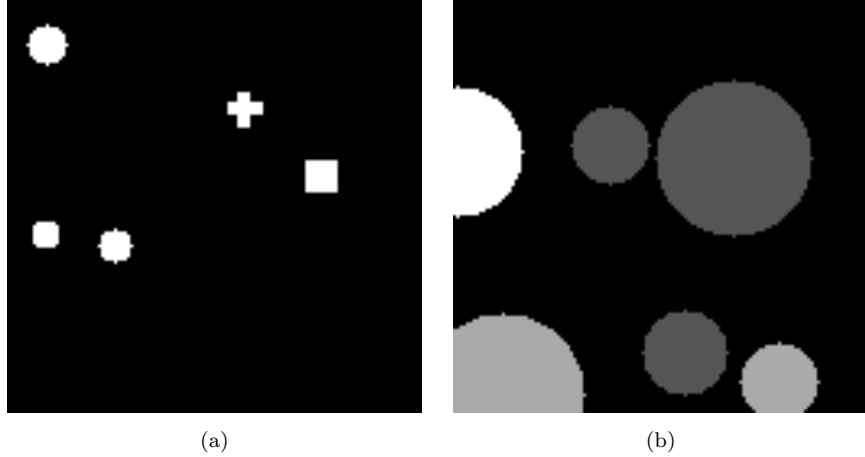


Figure 2: Example of an image from the dataset (a) AIXI-Shape and (b) AIXI-Color

These shapes were combined to form each image in the dataset. All the patterns had random sizes, positions, and appearances. Nonetheless, we define a set of restrictions:

- One image contained a maximum of two objects of the same pattern.
- We did not allow overlapping shapes.
- All patterns had the same intensity.

With the proposed methodology, we must define the function $g(p_i, I)$. As already explained this function obtains numerical data from the visual patterns of the images. Here, $g(p_i, I) = |p_i \in I|$. The position of these p_i in addition to the w_i given by the function used, allows the generation of a GT explanation for each pixel.

3.1.2. AIXI-Color

AIXI-Color, in contrast to AIXI-Shape, is a dataset containing only one type of shape, circles, but of different sizes and values. These circles have three possible intensity values, as shown in Figure 2b. This randomly defined intensity value is the pattern used for the attribution function. Similarly, the positions of the circles were randomized. The random position has only one constraint: the circles must not intersect.

We used the same $g(p_i, I)$ of the previous dataset. In addition to the weights of the functions, these features enabled, as already explained for the AIXI-Shape dataset, the generation of ground truth as a saliency map.

3.2. Functions

Following the proposed methodology, we must also define the attribution function F . All functions, as discussed in the previous section, must comply with a set of requirements. We define three different functions: *ssin*, *suum* and *class*.

3.2.1. SSIN

First proposed by Cortez and Embrechts [3] the *ssin* function (see equation 1), is defined as the sum of three factors based on the *sin* function. Each of these three factors has an associated weight, w_i . These weights were defined by the authors as *theoretical relative importance of* (0.55, 0.27, 0.18), *e.g.*, $0.55 = 0.5/(0.5 + 0.25 + 0.125)$. This function has one main restriction: the output of the associated function, $g(p_i, I)$, must be in the range $[0, 1]$. This range was defined because the maximum value of *sin* was obtained using $\pi/2$. Therefore, the maximum value for the *ssin* function was obtained when all factors had the maximum value of 1, essentially when x_1 , x_2 and x_3 were equal to $\pi/2$.

$$ssin(x) = 1/2 \cdot \sin(\frac{\pi}{2}x_1) + 1/4 \cdot \sin(\frac{\pi}{2}x_2) + 1/6 \cdot \sin(\frac{\pi}{2}x_3). \quad (1)$$

We adapted the original function to our methodology and notation as follows:

$$ssin(x) = w_1 \cdot \sin(\frac{\pi}{2}g(p_1, x)) + w_2 \cdot \sin(\frac{\pi}{2}g(p_2, x)) + w_3 \cdot \sin(\frac{\pi}{2}g(p_3, x)), \quad (2)$$

where $g(p_i, x)$ indicates some information of the image x regarding the patten p_i , and w_i is the weight for each factor, where $w_1 = 0.55$, $w_2 = 0.27$, $w_3 = 0.18$

This function aims to *mimic an additive response of independent nonlinear inputs*. The result was a continuous value between zero and one. For this reason, we considered this to be a regression task.

3.2.2. *SUUM*

We simplify the *ssin* function to verify whether our methodology can also work with a linear function. We call the resulting function *suum*:

$$suum(x) = w_1 \cdot g(p_1, x) + w_2 \cdot g(p_2, x) + w_3 \cdot g(p_3, x), \quad (3)$$

similar to the *ssin* function, the weights had the values $w_1 = 0.55$, $w_2 = 0.27$, $w_3 = 0.18$. The theoretical function outputs are in the range of $(-\infty, +\infty)$. We normalized the information output of $g(p_1, x)$ to be in the range $[0, 1]$; for this reason, the range of $suum(x)$ was also reduced to $[0, 1]$. Similar to the *ssin* function, we consider it a regression problem.

3.2.3. *Class*

We define a new function that allows us to simulate a classification problem. To accomplish this, we define a discrete function *class*. This function is defined as follows:

$$class(x) = w_1 \cdot g(p_1, x) - w_2 \cdot g(p_2, x) \geq 0, \quad (4)$$

where w_1 and w_2 are 1 and 0.5, respectively, $g(p_i, x)$ indicates numerical information regarding the visual patterns. We can see, that the function only considered two patterns the rest, if they existed, were ignored. Because the function has a threshold operation, the only possible values are 0 or 1. Furthermore, we considered the function of having semantic meaning. For example, if the $g(p_i, x)$ function indicates the number of occurrences of pattern p_i , then the function $class(x)$ is 1 when there are more objects of the first pattern than of the second. The fact that the output of the function was binary, led us to consider any model that estimates the function as a classification model.

3.3. *Predictive model*

As explained in previous sections, with this experimental setup, we aimed to verify the quality of the ground truth generated with the proposed methodology. To measure this quality, we must have something to compare it with. For this reason, we required two different elements: a predictive model and an XAI method. We used both for comparison with the proposed GT.

We define a predictive model as a function $f(x)$, where x is a 2D image and $f(x)$ is a prediction of the content of x . Explanations were extracted from the predictive model. We used two types of predictive model. First, we

used as the model directly the functions defined in section 3.2. Second, we used a deep learning model trained to approximate the same functions.

We used this function as a predictive model to avoid any possible errors in the prediction. We used the explanations obtained from this model as baseline punctuation which allowed us to identify the limitations of the successive model. Because it was not a real AI model, we could only use agnostic XAI methods. An agnostic method was defined in [12] as the method that *treat the original model as a black box*.

We also used a deep learning model to simulate a real scenario. Because deep learning models are universal function estimators [5], these types of models can learn any F that we had previously defined. If the model correctly estimated this function, necessarily also had learned the weight associated to each pattern. For this reason, we consider the w_i of each pattern the correct explanation for the result. We used a convolutional neural network (CNN), a special neural network for images-related tasks. The model was reintroduced by Krizhevsky *et al.* [6]. The authors proposed a model with two different parts: a convolutional part, responsible for pattern recognition, and a classification part, responsible for combining these recognized patterns into semantic information. The convolutional part was built with three main elements: convolutional layers, rectified linear unit (ReLU), and max pooling operations. The classification component was a multilayer perceptron (MLP) with a softmax operation as the activation function. All these building blocks were discussed in the original work. These model apply to classification and regression tasks.

We designed and trained a set of CNNs by following the basic structure proposed by Krizhevsky *et al.* [6]. We made minor modifications to the architecture to ensure that the value of the validation metrics was at least on the best decile. We needed to obtain good results to ensure that the AI model learned the desired F function.

The specific details of the implementation are beyond the scope of this study.

3.4. XAI method

Once we had defined the predictive models, we also needed to select the XAI method. We used an XAI method to obtain explanations and compare them to our ground truth. Because our goal was to verify the quality of the ground truth and not vice versa, we needed to ensure that the obtained

explanations were accurate. We defined a set of requirements to select the best XAI method according to them:

- **Verified.** The XAI method needed to be largely tested and verified to have the minimum number of unknown errors possible.
- **End to end.** The method must be able to analyse the entire AI model. This restriction was set because our proposal generated exact explanations.
- **Fidelity.** Fidelity, as explained in the previous section, is the similarity between the explanation obtained and the actual casual relation learned by the model. Because this experimental setup aimed to verify whether the generated ground truth was correct, we needed to extract the cause of the models with high accuracy to compare it to the ground truth. For this reason, the most important requirement was that the method had a high fidelity.

If a method fulfils these three requirements, the explanation obtained was accurate. The XAI method which complied more satisfactory these restriction was, Local Interpretable Model-agnostic Explanations (LIME).

LIME was first introduced by Ribeiro *et al.* [12]. The authors proposed building a local environment around a particular input using occlusions. This local environment of the solution space, allows learning simpler methods, interpretable by design, as a proxy for the underlying, more complex model to be explained.

We verified whether the LIME were complied with the requirements that we defined. First, this method had been widely used, tested, and verified, as demonstrated by over 5000 citations ¹ on *scopus*. Therefore, we considered that a major part of the limitation of the method was already discovered. Second, LIME considered the entire model and not only one part, as previously explained. Finally, the original authors discussed how, via a set of parameters, we could define the trade-off between fidelity and interpretability. Here, we maximized the fidelity of the method to ensure that the obtained results provided an exact explanation of the respective data.

¹Last time checked on 12-01-2022

3.5. Performance measures

The results of the explanation methods were measured and compared with the ground truth of the datasets. We proposed the use of well-defined metrics to assess the quality of explanations. Because we had an exact ground truth for each explanation, we considered the problem of extracting the explanation as a regression problem. For this reason, we used the following metrics for regression problems:

- **Mean absolute error (MAE).** MAE, or L1 Norm, is a common distance function:

$$MAE(X_e, Y) = \frac{\sum_{i=0}^n |X_{e_i} - Y_i|}{n}, \quad (5)$$

where X_{e_i} is the explanation obtained from the XAI method for the pixel i , and Y_i is the ground truth for the same i pixel in an image of n pixels.

- **Mean squared error (MSE).** MSE or L2 Norm is a standard distance function defined as follows:

$$MSE(X_e, Y) = \frac{\sum_{i=0}^n (X_{e_i} - Y_i)^2}{n}, \quad (6)$$

where X_{e_i} is the explanation obtained from the XAI method for the pixel i , and Y_i is the ground truth for the same i pixel in an image of n pixels.

Both distance functions have a range $[0, +\infty]$. With a perfect result of 0. The major difference between the two measures is that the MSE is more sensitive to outliers. Because we did not know a priori whether the results had outliers, we used both metrics.

3.6. Experiments

Two experiments were conducted to study the proposed methodology. The first experiment was characterized by the fact that we used the function itself instead of an AI model. In the second experiment, we used an AI model. Each of these two experiments had six sub-experiments each. Nonetheless, all of them share that they were built with the combination of one dataset and a function.

These experiments aimed to assess whether the GT generated by our methodology was in fact the correct ground truth.

In all experiments, we used LIME as the XAI method, to obtain explanations. We compared these explanations with the GT generated by our method. We used both metrics defined in Section 3.5.

In the first experiment, we used a function F as the predictor to avoid unexpected errors provoked by the AI model. Because we did not train any model, we could be sure that the prediction was perfect, and for this reason, we know that all errors were produced either by the XAI method or the proposed methodology. We considered the results obtained from these experiments as baseline results.

In the second experiment, we used an AI model. We use the model explained in Section 3.3. This experiment aimed to simulate a real scenario in a simplified manner. Similar to the first experiment, we extracted the explanations using LIME. The major caveat of using an AI model was the possibility of adding new errors without relation to our methodology.

The experiments were divided into six sub-experiment. Each of these six sub-experiments was defined by the dataset and function used, as presented in sections 3.1 and 3.2:

- **Sub-experiments *ssin*.** These experiments aimed to test the proposed methodology for the regression of non-linear functions. We defined two sub-experiments with different datasets that aimed to test this. We used, in both cases, the *ssin* function.

We used in the first sub-experiment the **AIXI-Shape** dataset and in the second the **AIXI-Color**. In both cases, the $g(p_i, I)$ used to calculate the *ssin* was $g(p_i, I) = |p_i \in I|$, indicating how many objects of the respective pattern were found on the image.

- **Sub-experiments *suum*.** These experiments were defined to assess whether our methodology was useful for the regression of linear functions. We used the same two datasets from the previous experiments. We used the *suum* function and again $g(p_i, I) = |p_i \in I|$.
- **Sub-experiments *class*.** These experiments were defined to assess whether our methodology was useful for classification tasks. We used the *class* function, defined in Section 3.2, and similarly to the previous experiments, both **AIXI-Shape** and **AIXI-Color** dataset and $g(p_i, I) = |p_i \in I|$.

4. Results and discussion

In this section, we discuss and analyse the results of the experiments defined in Section 3.6.

4.1. Experiment 1

Table 1 lists the results of the first experiment. The table summarizes the MAE and MSE for each sub-experiment and each p independently. The last column aggregates the results for each p into a single measurement. The experiment was designed to use the respective $F : \mathcal{X} \rightarrow \mathbb{R}$ function as the predictive model itself.

From the last column, we can observe that the overall quality of all experiments had similar values. We also see that the MSE value is always smaller than the respective MAE. This was because the units of MSE were squared with respect to MAE. Nonetheless, if we look closely at the results, taking into consideration not only the aggregated ones, but also the results for each pattern, we can see that in the sub-experiments that used the *class* function, the first two patterns had the worst results compared to the other sub-experiments. These results were at least one order of magnitude worse than the rest of the sub-experiments. This behaviour occurred because these two sub-experiments were based on classification tasks.

These worse results for classification tasks were provoked by the limitation of LIME. In a classification problem, if the perturbation of the input is not sufficiently large, the output will not vary. Nonetheless, even the results of the classification tasks had nearly perfect measures.

Based on the previous analysis, we can state that the proposed methodology generates the correct ground truth. Even so, there were sub-experiments with worse results, we expected that behaviour, and we assessed that it was provoked by the limitation of the XAI method used.

4.2. Experiment 2

Table 2 lists the results obtained in Experiment 2. Similar to the previous experiment, the table summarizes the MAE and MSE of all sub-experiments for all patterns, p . The last column aggregates the results for all patterns. This experiment used an AI model as the predictive model that estimates the respective $F : \mathcal{X} \rightarrow \mathbb{R}$ function.

The last column shows that the overall measurements of all experiments had similar values. We can see again that the MSE value was always smaller

| Function | Dataset | Measure | p_1 | p_2 | p_3 | Mean |
|--------------|------------|---------|--------|--------|--------|--------|
| <i>SSIN</i> | AIXI-Shape | MAE | 0.0034 | 0.0889 | 0.0939 | 0.0621 |
| | | MSE | 0.0001 | 0.0209 | 0.0009 | 0.0073 |
| | AIXI-Color | MAE | 0.0022 | 0.0339 | 0.0545 | 0.0302 |
| | | MSE | 0.0005 | 0.0045 | 0.0189 | 0.0079 |
| <i>SUUM</i> | AIXI-Shape | MAE | 0.0000 | 0.0056 | 0.0036 | 0.0031 |
| | | MSE | 0.0000 | 0.0000 | 0.0009 | 0.0003 |
| | AIXI-Color | MAE | 0.0016 | 0.0117 | 0.0578 | 0.0237 |
| | | MSE | 0.0005 | 0.0022 | 0.0189 | 0.0072 |
| <i>CLASS</i> | AIXI-Shape | MAE | 0.0114 | 0.1083 | 0.0006 | 0.0399 |
| | | MSE | 0.0008 | 0.0291 | 0.0000 | 0.0096 |
| | AIXI-Color | MAE | 0.0152 | 0.1435 | 0.0019 | 0.0535 |
| | | MSE | 0.0039 | 0.0396 | 0.0003 | 0.0146 |

Table 1: Results obtained for experiment 1. The columns p_1 , p_2 , p_3 show the results for each pattern. The last columns aggregate the independent elements.

than the respective MAE for the same reason. It also exhibited worse results for classification tasks. We expected this behaviour because the AI model, approximated function F , adding errors to the prediction.

| Function | Dataset | Measure | p_1 | p_2 | p_3 | Mean |
|--------------|------------|---------|--------|--------|--------|--------|
| <i>SSIN</i> | AIXI-Shape | MAE | 0.0139 | 0.0784 | 0.1007 | 0.0643 |
| | | MSE | 0.0018 | 0.0118 | 0.0190 | 0.0109 |
| | AIXI-Color | MAE | 0.0235 | 0.0620 | 0.0737 | 0.0530 |
| | | MSE | 0.0043 | 0.0097 | 0.0123 | 0.0087 |
| <i>SUUM</i> | AIXI-Shape | MAE | 0.0105 | 0.0505 | 0.1280 | 0.0630 |
| | | MSE | 0.0008 | 0.0061 | 0.0255 | 0.0108 |
| | AIXI-Color | MAE | 0.0245 | 0.0804 | 0.1122 | 0.0724 |
| | | MSE | 0.0052 | 0.0208 | 0.0522 | 0.0261 |
| <i>CLASS</i> | AIXI-Shape | MAE | 0.0138 | 0.1743 | 0.0006 | 0.0629 |
| | | MSE | 0.0014 | 0.0588 | 0.0036 | 0.0213 |
| | AIXI-Color | MAE | 0.0336 | 0.1499 | 0.0241 | 0.0692 |
| | | MSE | 0.0124 | 0.0452 | 0.0154 | 0.0243 |

Table 2: Results obtained for experiment 2. The columns p_1 , p_2 , p_3 show the results for each pattern. The last columns aggregate the independent elements.

Based on the previous analysis, we can state that our methodology is

correct. The fact that the results of the second experiment were similar to those of the first one indicated that the AI model approximates the function F . The above demonstrates that our assumptions hold: when we used the proposed methodology, the GT generated was the actual cause for the predictions for the AI models.

5. Conclusion

In this study, we propose a novel methodology to generate a SAB dataset of images. Our methodology allowed use to define the precise importance for each pixel of an image and can be used for generalist problems, such as classification and regression. This ground truth allowed us to ignore the ad hoc solutions proposed in the state-of-art.

Compared with previous approaches for evaluating the quality of XAI methods, we accomplished a perfect GT. We verified this using two different experiments, both in a controlled environment. We obtained explanations using LIME to verify whether our GT was correct. We used this algorithm because its results achieved high fidelity. Our GT was very similar to the LIME results therefore, we can state that we generated the correct ground truth. This allows us to use our GT to measure the quality of any XAI method.

We included as results the implemented code for the generation of the datasets (see <https://github.com/miquelmn/aixi/releases/tag/1.0.0>). As an additional contribution we constructed and opened to the scientific community two synthetic datasets, AIXI-Color and AIXI-Value, with the positions of the objects and their classes as a ground truth. For the sake of scientific progress, it would be beneficial if authors published their raw data, code, and the image datasets.

Using this methodology for others XAI algorithms would allow the measurement of its actual fidelity without making any untested assumptions and avoiding any bias. Nonetheless, we consider the application of this methodology to the rest of algorithms a future work.

6. Declaration of competing interest

The authors declare that they have no known competing financial interests or personal relationships that could have influenced the work reported in this study.

7. Author contributions

Conceptualization: M.M.-N., G.M.-A., and A.J.-i.-C.; methodology: M.M.-N., G.M.-A., and A.J.-i.-C.; validation: M.M.-N., G.M.-A., and A.J.-i.-C.; formal analysis: M.M.-N., G.M.-A., and A.J.-i.-C.; resources: G.M.-A. and A.J.-i.-C.; data curation: M.M.-N.; writing—original draft preparation: M.M.-N.; writing—review and editing: M.M.-N., G.M.-A., and A.J.-i.-C.; supervision: G.M.-A. and A.J.-i.-C.; project administration: A.J.-i.-C.; funding acquisition: A.J.-i.-C. All authors have read and agreed to the published version of the manuscript.

8. Funding

Project PID2019-104829RA-I00 “EXPLainable Artificial INtelligence systems for health and well-beING (EXPLAINING)” funded by MCIN/AEI/10.13039/501100011033. Miquel Miró-Nicolau benefited from the fellowship FPI_035.2020 from Govern de les Illes Balears.

References

- [1] D. Alvarez-Melis and T. S. Jaakkola. Towards Robust Interpretability with Self-Explaining Neural Networks. *Advances in Neural Information Processing Systems*, 2018-Decem(NeurIPS):7775–7784, jun 2018. ISSN 10495258. URL <http://arxiv.org/abs/1806.07538>.
- [2] L. Arras, A. Osman, and W. Samek. Clevr-xai: A benchmark dataset for the ground truth evaluation of neural network explanations. *Information Fusion*, 81:14–40, 2022. ISSN 1566-2535. doi: <https://doi.org/10.1016/j.inffus.2021.11.008>. URL <https://www.sciencedirect.com/science/article/pii/S1566253521002335>.
- [3] P. Cortez and M. J. Embrechts. Using sensitivity analysis and visualization techniques to open black box data mining models. *Information Sciences*, 225:1–17, 2013. ISSN 0020-0255. doi: <https://doi.org/10.1016/j.ins.2012.10.039>. URL <https://www.sciencedirect.com/science/article/pii/S0020025512007098>.
- [4] T. Gomez, T. Fréour, and H. Mouchère. Metrics for saliency map evaluation of deep learning explanation methods. pages 1–12, jan 2022. URL <http://arxiv.org/abs/2201.13291>.

- [5] K. Hornik, M. Stinchcombe, and H. White. Multilayer feedforward networks are universal approximators. *Neural networks*, 2(5):359–366, 1989.
- [6] A. Krizhevsky, I. Sutskever, and G. E. Hinton. Imagenet classification with deep convolutional neural networks. *Advances in neural information processing systems*, 25, 2012.
- [7] A. Mamalakis, E. A. Barnes, and I. Ebert-Uphoff. Investigating the fidelity of explainable artificial intelligence methods for applications of convolutional neural networks in geoscience. *Artificial Intelligence for the Earth Systems*, 1(4):e220012, 2022.
- [8] T. Miller. Explanation in artificial intelligence: Insights from the social sciences. *Artificial intelligence*, 267:1–38, 2019.
- [9] M. Miró-Nicolau, G. Moyà-Alcover, and A. Jaume-i Capó. Evaluating explainable artificial intelligence for x-ray image analysis. *Applied Sciences*, 12(9):4459, 2022.
- [10] V. Petsiuk, A. Das, and K. Saenko. RISE: Randomized Input Sampling for Explanation of Black-box Models. *British Machine Vision Conference 2018, BMVC 2018*, 1, jun 2018. URL <http://arxiv.org/abs/1806.07421>.
- [11] L. Qiu, Y. Yang, C. C. Cao, Y. Zheng, H. Ngai, J. Hsiao, and L. Chen. Generating perturbation-based explanations with robustness to out-of-distribution data. In *Proceedings of the ACM Web Conference 2022*, pages 3594–3605, 2022.
- [12] M. T. Ribeiro, S. Singh, and C. Guestrin. ” why should i trust you?” explaining the predictions of any classifier. In *Proceedings of the 22nd ACM SIGKDD international conference on knowledge discovery and data mining*, pages 1135–1144, 2016.
- [13] W. Samek, A. Binder, G. Montavon, S. Lapuschkin, and K.-R. Muller. Evaluating the Visualization of What a Deep Neural Network Has Learned. *IEEE Transactions on Neural Networks and Learning Systems*, 28(11):2660–2673, nov 2017. ISSN 2162-237X. doi: 10.1109/TNNLS.2016.2599820. URL <https://ieeexplore.ieee.org/document/7552539/>.

- [14] R. Tomsett, D. Harborne, S. Chakraborty, P. Gurram, and A. Preece. Sanity checks for saliency metrics. In *Proceedings of the AAAI conference on artificial intelligence*, volume 34, pages 6021–6029, 2020.
- [15] B. H. van der Velden, H. J. Kuijf, K. G. Gilhuijs, and M. A. Viergever. Explainable artificial intelligence (XAI) in deep learning-based medical image analysis. *Medical Image Analysis*, 79:102470, jul 2022. ISSN 13618415. doi: 10.1016/j.media.2022.102470. URL <http://arxiv.org/abs/2107.10912><https://linkinghub.elsevier.com/retrieve/pii/S1361841522001177>.